Resolution and Mass Accuracy in Matrix-Assisted Laser Desorption Ionization-Time-of-Flight

Marvin Vestal and Peter Juhasz
PerSeptive Biosystems, Framingham, Massachusetts, USA

A mathematical model of time-of-flight mass analyzers employing uniform electric fields is presented that allows "exact" calculations of flight times as functions of mass-to-charge ratio, initial velocity and position, applied voltages, and instrument geometry. An "approximate" equation based on a series expansion of the "exact" result is derived which allows focusing conditions and limits on resolution to be determined for different instrument geometries and operating conditions. The fundamental theory is applied to predicting resolution and mass accuracy in matrix-assisted laser desorption ionization-time of flight. In this case higher order velocity focusing can provide excellent correction for the initial velocity distribution of a selected mass-to-charge ratio, but the focusing is mass-to-charge ratio dependent. There is generally a trade-off between ultimate resolution at a particular mass-to-charge ratio and resolution and mass accuracy over a broad mass range. In most practical applications the latter is more important. Calculations are compared with experimental results for a particular analyzer geometry, both at theoretical optimum velocity focus and at operating conditions where ultimate resolution is sacrificed for a broader range of relatively high resolution and better mass accuracy. (J Am Soc Mass Spectrom 1998, 9, 892–911) © 1998 American Society for Mass Spectrometry

In early applications of matrix-assisted laser desorption ionization-time-of-flight (MALDI-TOF) using either reflecting [1] or linear [2] TOF analyzers, the mass resolution was poor and the mass accuracy was limited. It was soon noted [3, 4] that the major limitation on resolution and mass accuracy was imposed by the relatively broad distribution of initial velocities for ions produced by MALDI. More recently, delayed extraction techniques [5–8] have been developed that minimize the effect of initial ion velocity and allow much better resolution and mass accuracy to be obtained with MALDI-TOF.

In this article a mathematical model of systems employing uniform electric fields is presented which allows "exact" calculations of flight times as functions of mass-to-charge ratio, initial velocity and position, applied voltages, and instrument geometry. An "approximate" equation based on a series expansion of the exact result is derived which allows focusing conditions and limits on resolution to be determined for different instrument geometries and operating conditions. Focusing conditions can be determined for either the case where spatial spread of the initial ion packet is relatively large and the velocity spread small (such as in orthogonal injection systems) or in the case where velocity spread is large and ions are ejected from a flat surface (e.g., MALDI). Specific examples discussed include space (energy) and velocity focusing with the two-stage source of Wiley and McLaren [9] and with a system employing a single-stage source with a single-stage mirror.

The fundamental theory is applied to predicting resolution and mass accuracy in MALDI-TOF. In this case higher order velocity focusing can provide excellent correction for the initial velocity distribution of a selected mass-to-charge ratio, but the focusing is mass-to-charge ratio dependent. There is generally a trade-off between ultimate resolution at a particular mass-to-charge ratio and resolution and mass accuracy over a broad mass range. In most practical applications the latter is more important. Calculations are compared with experimental results for two analyzers, both at theoretical optimum velocity focus and at operating conditions where ultimate resolution is sacrificed for a broader range of relatively high resolution and better mass accuracy.

Theory

As discussed in detail in Appendix I, equations for calculating the TOF of an ion through any system

Address reprint requests to Marvin Vestal, PerSeptive Biosystems, 500 Old Connecticut Path, Framingham, MA 01701.

1044-0305/98/$19.00
PII S1044-0305(98)00069-5

Received March 10, 1998
Revised May 26, 1998
Accepted May 26, 1998

involving uniform electric fields can be derived from the laws of basic physics. Such equations can be used to accurately determine the flight time as a function of mass-to-charge ratio for any specific instrument provided the distances, voltages, and initial conditions are given. In general, the accuracy of such calculations is limited only by uncertainties in the precise values of the input parameters and by the extent to which the simplified one-dimensional model accurately represents the real three-dimensional instrument. Unfortunately, the exact equations are difficult to use in designing systems that provide optimum performance for particular applications. For any combination of uniform electric fields, the exact equation for TOF can be approximated by the expression

$$t = (Df_0/v_n)[1 + f_1p/f_0 + f_2p^2/f_0 + f_3p^3/f_0 + \cdots - (2d_ay/f_0D)(v_0/v_n)] \quad (1)$$

where D is the length of the field-free region, d_a is the length of the first ion acceleration region, v_0 is the initial velocity of the ion, v_n is the velocity of an ion of a particular mass-to-charge ratio after it is accelerated from rest through the total accelerating potential V, and y is the ratio of the total accelerating potential to the portion applied across the first accelerating region. All of the details of the analyzer geometry and relative operating voltages are contained in the dimensionless coefficients f_0, f_1, f_2, f_3, and explicit expressions for all of the common configurations, including one- and two-field ion sources and mirrors, are given in Appendix I. The dimensionless perturbation p is explicitly the energy deficit of an ion produced at position x, with initial velocity v_0, divided by the nominal kinetic energy after the first stage of acceleration.

The dependence on mass-to-charge ratio of the ions is contained in the expressions for v_n and p. Namely,

$$p = x/d_a - yT_0/zV = x/d_a - y(v_0/v_n)^2 \quad (2)$$

$$v_n = (2zV/m)^{1/2} \quad (3)$$

$$T_0 = mv_0^2/2 \quad (4)$$

The accuracy of eq 1 is limited only by truncation of the power series in the perturbation p. If the power series were continued to infinity, eq 1 would be exactly equivalent to the exact equation from which it was derived. The last term in eq 1, which depends on the first power of the initial velocity, is exact for all cases. For most of the applications considered in this paper the perturbation p is on the order of 1% or less, and the error induced by truncating after the cubic term is less than 1 ppm. If higher accuracy is required, or if p is larger, then more terms must be added to the expansion.

The utility of eq 1 can perhaps be seen more clearly by rewriting it in the form

$$t = t_n[(1 + \epsilon(x, v_0)] \quad (5)$$

where

$$t_n = Df_0/v_n \quad (6)$$

$$\epsilon(x, v_0) = f_1p/f_0 + f_2p^2/f_0 + f_3p^3/f_0 + \cdots - (2d_ay/f_0D)(v_0/v_n) \quad (7)$$

Or, rearranging eq 5

$$\epsilon(x, v_0) = (t - t_n)/t_n \quad (8)$$

Thus, the nominal flight time t_n of a particular ion is given by the effective flight distance Df_0 divided by the nominal velocity v_n and the distribution of flight times relative to the nominal is given by $\epsilon(x, v_0)$. If the distributions of initial position and velocity are known, then the detailed flight time distribution for an ion of any specified mass-to-charge ratio can be calculated using the above equations.

Focusing Conditions

Focusing in TOF mass spectrometry involves minimizing the dependence of the flight time on initial conditions. The general condition for focusing to a particular order is that the derivative of the quantity in question (in this case the TOF) with respect to the variable in question (the initial position or velocity) vanishes at the mean of the distribution of the variable. For first order focusing the first derivative must be zero; for second order focusing, both the first and second order derivatives must simultaneously vanish, and so on. It is well known from the work of Wiley and McLaren [9] and others, that it is not possible to cause the first derivatives of flight time with respect to both velocity and position to vanish simultaneously. Thus, depending on the relative widths of the distributions, one may choose to employ space focusing when the velocity distribution is narrow, and velocity focusing when the spatial distribution is narrow. In some cases, such as orthogonal injection or gas phase ionization in the TOF ion source, the ratio v_0/v_n is small and independent of mass-to-charge ratio, and the challenge is to reduce the dependence on initial position x. This is normally termed "space" focusing, but it should be noted that it is in reality "energy" focusing. In other cases, such as MALDI, the initial velocity may be large and nearly independent of mass-to-charge ratio, but the ions are produced from a planar surface with a small variation in initial position. In this case velocity focusing is required.

For determining space focusing conditions we as-

sume that the initial velocity is negligible. In this case we have

$$\epsilon(x, v_0 = 0) = f_1(x/d_a)/f_0 + f_2(x/d_a)^2/f_0 + f_3(x/d_a)^3/f_0 + \cdots \quad (9)$$

Space focusing to a particular order is achieved by causing the corresponding coefficient in the power series in x/d_a to vanish. Thus, first order space focusing requires that f_1 vanish, and second order space focusing requires that both f_1 and f_2 vanish simultaneously. Actually, this is energy focusing because the dependence on initial kinetic energy as well as on initial potential energy is minimized by this focusing. Space focusing has no effect on the last term in eq 1 or 7, which is proportional to the first power of the initial velocity, and in many cases this may be the dominant term limiting resolution under these conditions.

Velocity focusing requires minimizing the dependence of flight time on initial velocity, including the first power term. As was discussed originally by Wiley and McLaren [9], this can be accomplished by delaying the application of the accelerating field. If ions are produced in a field-free region and application of the first acceleration field is delayed for some time Δt after ion formation, then the position of the ions at the time of application of the field is given by

$$x = v_0 \Delta t \quad (10)$$

If eq 1 is rewritten as a power series in the initial velocity, then velocity focusing to a particular order is achieved by causing the corresponding coefficient in the power series to vanish. If the variation in initial position is small, and delayed extraction is employed, then the perturbation p is given by

$$p = x/d_a - yT_0/zV = v_0 \Delta t/d_a - y(v_0/v_n)^2 \quad (11)$$

Substituting this expression for p in eq 1 and rearranging into a power series in v_0, the flight time may be expressed approximately as

$$t = (Df_0/v_n)[1 + h_1 q + h_2 q^2 + h_3 q^3 + \cdots] \quad (12)$$

where

$$q = v_0/v_n \quad (13)$$

and

$$h_1 = (f_1\tau - 2d_a y/D)/f_0 \quad (14)$$

$$h_2 = (f_2\tau^2 - f_1 y)/f_0 \quad (15)$$

$$h_3 = (f_3\tau^3 - 2f_2\tau y)/f_0 \quad (16)$$

The dimensionless parameter τ is proportional to the delay time and is given by

$$\tau = v_n \Delta t/d_a \quad (17)$$

This form of the TOF equation is useful for calculating focusing conditions and resolution limits when velocity focusing is required. Thus, first order velocity focusing requires $h_1 = 0$, and second order velocity focusing requires that both h_1 and h_2 vanish simultaneously.

Thus, the condition for first order velocity focusing is given by

$$f_0 h_1 = f_1 v_n \Delta t/d_a - 2d_a y/D = 0 \quad (18)$$

or

$$\Delta t = 2d_a^2 y/f_1 D v_n \quad (19)$$

The condition for simultaneous second order velocity focusing is given by

$$f_0 h_2 = f_2(v_n \Delta t/d_a)^2 - f_1 y = 0 \quad (20)$$

After substituting eq 19 for Δt this simplifies to

$$f_2 = (f_1^3/y)(D/2d_a)^2 \quad (21)$$

The time delay for first order focusing is proportional to the square root of the mass-to-charge ratio, but the second order focusing condition is independent of mass and depends only on the geometry and relative operating voltages. A necessary condition for first order velocity focusing is that the coefficient f_1 must be positive, and for second order velocity focusing both f_1 and f_2 must be positive. These requirements limit the range of source dimensions and operating conditions that can be used. Strictly speaking, these focusing conditions correspond to minimizing the dependence of flight times on initial velocity for distributions centered on zero. For cases such as MALDI where the average initial velocity is not zero, more accurate focusing conditions can be derived by minimizing flight time variation about the appropriate average initial velocity. In this case the derivatives should be evaluated at the average velocity. Using eq 12 this implies that the more precise focusing conditions are

$$h_1 + 2h_2 q + 3h_3 q^2 + \cdots = 0, \text{ first order} \quad (22)$$

$$h_2 + 3h_3 q + \cdots = 0, \text{ second order} \quad (23)$$

For most cases of practical interest the h coefficients are less than unity; thus the error in determining focusing conditions using 19 and 21 is less than q, where q is calculated from eq 13 using the average value of the initial velocity. For example, if $v_0 = 300$ m/s, then q is approximately 0.01 for an ion of m/z 5000 accelerated

to 20 kV. Since q is proportional to the square root of the mass, q is about 0.1 at m/z 500,000 and 0.001 at m/z 50. In any case, use of the simple focusing conditions $h_1 = 0$, first order, and $h_1 = h_2 = 0$, second order, provides a useful first pass at the appropriate focusing conditions, which allows the geometry to be optimized. If necessary the delay time then can be adjusted to satisfy eq 22 when more precise focusing is required.

Resolution

In TOF mass spectrometry the resolution is

$$R = \delta m/m = 2\delta t/t \tag{24}$$

where t is the flight time and δt is the peak width. Resolution is typically expressed in ppm and resolving power is the inverse. In TOF-MS peak widths are generally reported as full-width at half-maximum (FWHM), and resolutions are reported with the corresponding convention. If the initial distribution of ion positions and velocities is known, then the resolution of any particular configuration can be estimated using eq 1 with the appropriate focusing conditions. Normally, the resolution is approximately determined by the lowest order nonzero term in eq 1, but in cases near a focus where the leading term is small, it may be necessary to take the first two terms to provide an accurate estimate. In general, we can calculate a resolution limit R_s because of spatial spread, and separately a resolution limit R_v because of velocity spread. If these two contributions are independent, then the overall estimate of resolution is given by

$$R = (R_s^2 + R_v^2)^{1/2} \tag{25}$$

In cases such as orthogonal injection from an external source the initial velocity v_0 may be small and the perturbation is given by

$$p = \delta x/d_a \tag{26}$$

where δx is the width (FWHM) of the orthogonal beam. With first order space focusing, $f_1 = 0$, the space resolution limit, estimated from the second order term in eq 1 or 9, is

$$R_{s2} = 2f_2p^2/f_0 = 2(f_2/f_0)(\delta x/d_a)^2 \tag{27}$$

and the velocity resolution limit, given by the uncompensated first order velocity term, is

$$R_{v1} = 2(2d_ay/f_0D)(\delta v_0/v_n) \tag{28}$$

where δv_0 is the width of the velocity distribution (FWHM). When both first and second order space focusing are achieved, $f_1 = 0$, $f_2 = 0$, the space resolution is estimated from the third order term that is given by

$$R_{s3} = 2f_3p^3/f_0 = 2(f_3/f_0)(\delta x/d_a)^3 \tag{29}$$

and the velocity resolution is the same as above. In many cases the gain in overall resolution achieved by higher order space focusing may be small because the remaining first-order velocity resolution term is dominant, even though the velocity spread is relatively small.

In cases such as desorption of ions from surfaces, with delayed application of the accelerating field, the perturbation is given by

$$q = \delta v_0/v_n \tag{30}$$

and the term involving the initial position is small enough to be neglected in estimating the resolution defined by the velocity spread.

With first order velocity focusing the resolution limit due to initial velocity is given approximately by the second order velocity term in eq 12 after substitution of 30 for q, which is

$$R_{v2} = 2h_2q^2 = 2(\delta v_0/v_n)^2[f_2(2d_ay/f_1D)^2 - f_1y]/f_0 \tag{31}$$

and with first and second order velocity focusing the resolution is

$$R_{v3} = 2h_3q^3 = 2(\delta v_0/v_n)^3 \times [f_3(2d_ay/f_1D)^3 - 2f_2y(2d_ay/f_1D)]/f_0 \tag{32}$$

With velocity focusing the spatial resolution is given by the uncompensated first order term in eq 1 after substitution of 26 for p, which is

$$R_{s1} = 2f_1p/f_0 = 2(f_1/f_0)(\delta x/d_a) \tag{33}$$

By appropriate choice of operating conditions, as discussed above, the first order term in velocity can be set to zero for a particular value of mass-to-charge ratio, but for masses differing significantly from the focused mass the velocity limit on resolution is set by the residual uncompensated first order velocity dependence. From eq 1 this first order dependence is given by

$$R_m = R_{v1f}[1 - (m_f/m)^{1/2}] \tag{34}$$

where m_f is the mass corresponding to the first order focus, and R_{v1f} is the resolution limit in the absence of first order velocity focusing given by eq 28 evaluated at the focused mass. In all of the above equations for resolution limits the absolute value of the quantity in the square bracket is implied.

These equations can be used to estimate the theoretical resolution for any particular instrumental configuration, provided the initial distributions are known or can be estimated with reasonable accuracy. The theoretical estimate of resolution can be improved by using more terms from eq 1, but such corrections are only significant near a focal condition in which the leading term is small. In such cases the calculated contribution to peak width is generally very small, so that the practical resolution limit is set by other contributions to the peak width, and more accurate determination of a term which is not limiting resolving power is of little practical value.

Case I. Single-Stage Source with Drift Tube

This system consists of a uniform electrical field and a field-free drift space as illustrated in Figure 13 in the Appendix. In this case $y = 1$, and the f coefficients are given by eqs 88–92 in the Appendix. First order space focusing is satisfied by the geometrical condition

$$2d_a = D \tag{35}$$

and higher order space focusing is not possible. For first order velocity focusing we have from eq 19

$$\Delta t = 2d_a^2/f_1 D v_n \tag{36}$$

and second order velocity focusing, according to eq 21, requires that

$$[3 - 2d_a/D]/8 = \{[1 - 2d_a/D]/2\}^3 (D/2d_a)^2 \tag{37}$$

This is satisfied by the condition

$$6d_a = D \tag{38}$$

which implies that

$$f_0 = 4/3, \quad f_1 = f_2 = 1/3, \quad f_3 = 7/24 \tag{39}$$

and with this geometry the first order focusing condition becomes

$$\Delta t = d_a/v_n \tag{40}$$

The fact that both first and second order velocity focusing is possible with such a simple system is somewhat surprising, and to the best of our knowledge has not been noted previously; however, as discussed below, this analyzer has very limited practical utility.

For the purpose of comparing performance of different geometries for similar initial conditions, we will set the length of the field-free region, $D = 1$ m, and adjust the other parameters to achieve the desired focusing. In MALDI the initial velocity distribution is nearly independent of the mass of the analyte, but depends on the choice of matrix [15] and may depend on operating conditions such as laser intensity. For the purpose of comparing the performance of different analyzers we assume the average initial velocity is $v_0 = 300$ m/s and that the width of the velocity distribution (FWHM) is approximately equal to the average and is independent of the mass of the ion. In MALDI the uncertainty in initial position is small and may depend primarily on the size of the crystals produced on the surface. For the purpose of comparisons we assume $\Delta x = 10^{-2}$ mm. For this purpose we must also consider a particular mass and accelerating voltage. For this discussion we will take m/V equal to 1 Da/V, then v_n is approximately 13,800 m/s. This corresponds, for example, to an ion of m/z 20,000 Da accelerated by a potential difference of 20 kV. With first and second order velocity focusing the velocity limit on resolution is given by eq 32 and the spatial limit on resolution is given by eq 33, Thus

$$R_{v3}^{-1} = (16/9)(v_n/\delta v_0)^3 = 196{,}600$$

and

$$R_s^{-1} = 2(d_a/\delta x) = 33{,}300$$

This resolving power is achieved for $m/V = 1$ when application of the accelerating field is delayed from ion formation by

$$\Delta t = d_a/v_n = 1/(6 \times 13{,}800) \text{ s} = 12.08\ \mu\text{s}$$

and the appropriate delay for other masses is this value multiplied by the square root of m/V.

In space focusing applications, the strong dependence on initial velocity is an obvious limitation of this simple geometry. On the other hand, the resolution in the velocity focusing mode is excellent at the focused mass. The major problems with this simple analyzer are (1) the second order focus is entirely determined by the geometry and no electrical adjustment is possible, and (2) the focal conditions are very strongly mass dependent so that both high resolution and mass accuracy are achieved only over a relatively narrow mass range. The breadth of focus can be increased at the expense of maximum resolution at a particular mass by shortening the source relative to that satisfying second order focusing.

Case II. Single-Stage Source with Single-Stage Mirror

In this case the f coefficients are given by eqs 97–101 and the potential diagram for the single-stage mirror is shown in Figure 13c in the Appendix. First order space focusing is satisfied by the geometrical condition

$$2d_a + 4d_R = D \tag{41}$$

and higher order space focusing is not possible. The relative length of either the source or the mirror is not restricted by this condition, one may be treated as a free parameter and the other must be chosen to satisfy eq 41. First order velocity focusing is formally the same as for the single-field source without the mirror, eq 36, but now the length of the source relative to the drift distance may be varied. Second order velocity focusing requires that eq 21 be satisfied. If we let $r = 4d_R/D$, then this equation, which is quadratic in the parameter $2d_a/D$, can be solved to give

$$2d_a/D = [3(1 - r)^2/4r]\{[1 + 8r/9(1 - r)]^{1/2} - 1\} \quad (42)$$

Second order velocity focusing can be achieved by combinations of source and mirror lengths which satisfy eq (42). Results are summarized in Figure 1 where the relative source length and f coefficients for second order velocity focusing are plotted as a functions of mirror length. The left-hand side of the figure corresponds to the linear analyzer with no mirror. Also shown are the delay time for first order focusing, calculated resolving power limits R_{v3}^{-1}, R_{s1}^{-1} for $m/V = 1$ u/V, and R_{v1}^{-1} which determines the mass dependence of the resolving power. As can be seen from the figure, the limitation on resolving power is determined primarily by the spatial limit on resolving power since the velocity limit is much higher under all conditions. It should also be noted that addition of the mirror actually causes a decrease in the theoretical maximum resolving power, although this decrease is relatively minor until the source length becomes very small. The advantage of using the mirror is not better resolution at a given mass, but rather better resolution over a wide mass range, and better mass accuracy resulting from smaller dependence on the initial velocity of the ions. Results comparing resolution for the linear analyzer with that for the reflector at $r = 0.9$ are given in Figure 2. These results correspond to first and second order velocity focusing at $m/V = 1$ u/V. As can be seen from the figure, the theoretical resolving power for the linear analyzer at the focused mass is nearly twice that of the reflector, because of a higher spatial resolving power limit, but the range over which the linear analyzer gives higher resolving power is only about 1% of the focused mass.

Physical interpretation of the focusing conditions for space (energy) focusing is relatively simple. The field-free drift length is equal to the focal length of the source plus the focal length of the mirror. With delayed extraction velocity focusing, the source focal length can be adjusted by adjusting the delay time. When the source first-order velocity focus is made to coincide with the object plane of the mirror, then first order velocity focusing is also achieved at the detector. It should be noted that the mirror focusing is first order in energy; that is, the focusing properties are independent

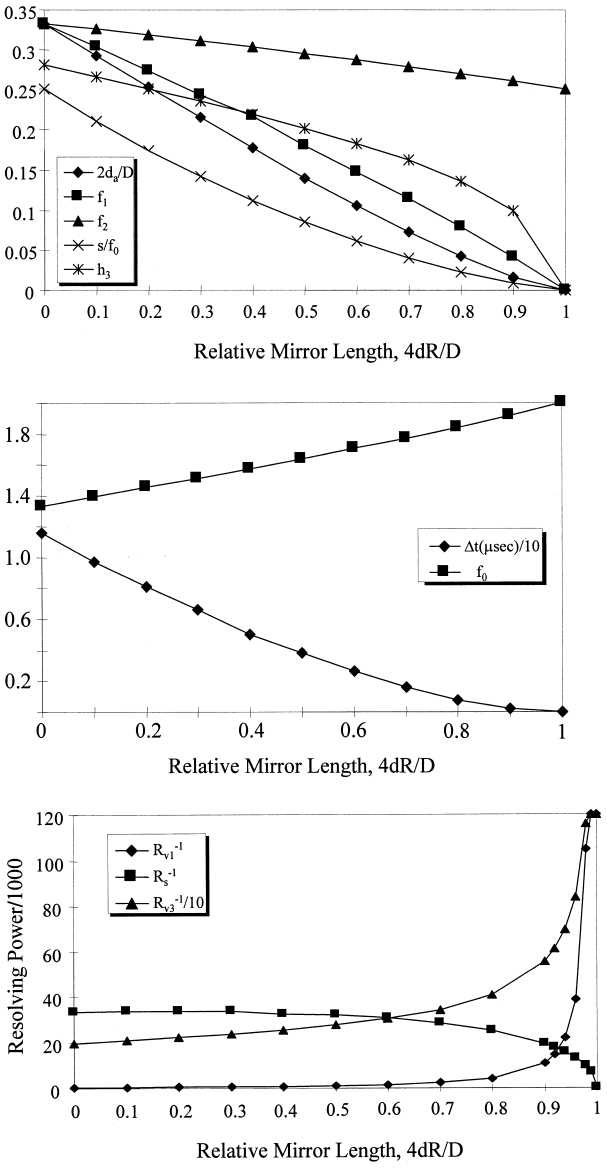

Figure 1. Summary of calculations on TOF analyzer consisting of single-stage source with single-stage mirror employing second order velocity focusing. In panel (**a**) the parameters $s = 2d_a/D$, f_1, f_2, s/f_0, and h_3 are plotted as functions of the relative mirror length $r = 4d_R/D$. Panel (**b**) shows the parameter f_0, where f_0D is the effective length of the analyzer, and the delay time Δt. Panel (**c**) shows the resolving power limits R_{s1}^{-1}, R_{v1}^{-1}, and R_{v3}^{-1}. Note that R_{v3}^{-1} is reduced by a factor of 10 to bring it on scale with the others. These calculations are based on a field-free distance, $D = 1$ m with $m/V = 1$ u/V and $v_0 = 300$ m/s.

of mass-to-charge ratio, but the first order velocity focusing is mass dependent. When both the first and second order focusing conditions are satisfied simultaneously, eqs 19 and 21, then both first and second order foci occur at the detector. The second order velocity focus is independent of mass-to-charge ratio. Second order focusing depends only on the geometry of the system. With the system consisting only of a single-field source and a field-free drift space, second order focusing occurs at a drift distance which is six times the

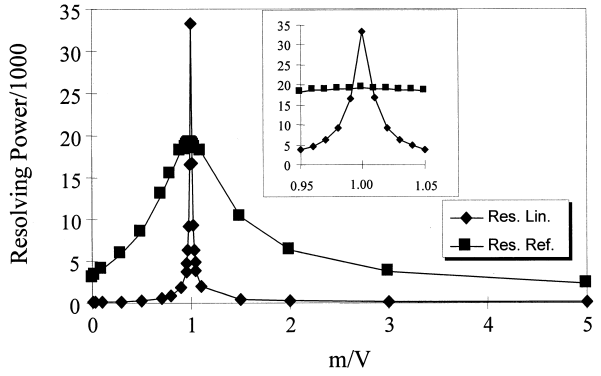

Figure 2. Calculated resolving power as a function of m/V with second order velocity focus at $m/V = 1$ for single-stage source, and for single-stage source with single-stage mirror, relative length $r = 0.9$, both with 1 m field-free drift space. Average initial velocity = 300 m/s. The region around the focused mass is blown up in the inset.

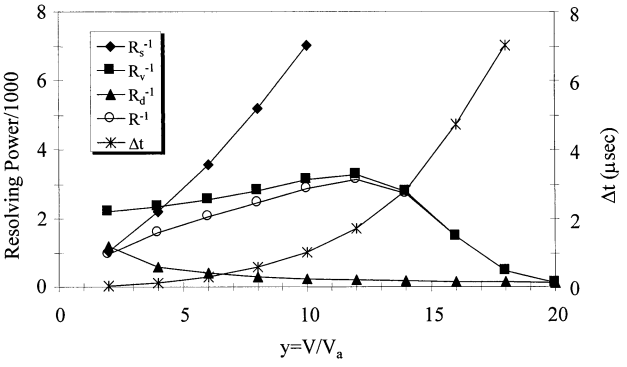

Figure 3. Calculated resolving power limits as functions of the voltage ratio y for a two-stage source with equal accelerating distances, $d_a = d_0 = 5$ mm, and 1 m field-free drift space with first order velocity focusing for $m/V = 1$, $v_0 = 300$ m/s. Shown are R_{s1}^{-1}, R_{v1}^{-1}, R_{v2}^{-1}, resultant resolving power R^{-1} and the delay time Δt producing first order focusing.

source length, and there are no adjustable parameters. To achieve both first and second order focusing the delay time is adjusted to cause the first order focus for a selected mass-to-charge ratio to occur at this distance. The addition of a mirror to this system provides a free parameter, the effective length of the mirror, which can be adjusted by changing the voltage applied to the back of the mirror. This combination allows a much shorter source to be used, and the mirror length can be adjusted to bring the second order focus to the detector. If the delay time is chosen to satisfy eq 19 for a particular nominal velocity, which depends on mass-to-charge ratio and the accelerating voltage, then the first and second order foci can be made to coincide for that value of mass-to-charge ratio.

Case III. Two-Stage Source with Drift Tube

The two stage source provides an additional free parameter, the voltage ratio y, which can be varied to adjust the focal length of the source. The potential diagram for the two-stage source is shown in Figure 13b in the Appendix. In this case the f coefficients are given by eqs 118–121 in the Appendix. The condition for first order space focusing, corresponding to $f_1 = 0$, is given by

$$\begin{aligned} 2d_a/D &= 1/y^{3/2} - (2d_0/D)[y^{1/2}/(y-1)] \\ &\quad \times (1/y - 1/y^{1/2}) \\ &= 1/y^{3/2} + (2d_0/D)/(y + y^{1/2}) \end{aligned} \tag{43}$$

which can be rearranged to the form

$$D = 2d_a y^{3/2}[1 - (d_0/d_a)/(y + y^{1/2})] \tag{44}$$

This is the focusing condition originally derived by Wiley and McLaren [9]. They also noted that second order focusing can also be achieved with a two-stage source. Setting both f_1 and f_2 equal to zero and eliminating d_a gives

$$2d_0/D = 1 - 3/y \tag{45}$$

which must be satisfied simultaneously with the first order condition (43)

The conditions required for first and second order velocity focusing, eqs 19 and 21 above can be satisfied by a range of values of the relative source lengths with a specific value for the voltage ratio y for each geometry. Unfortunately, the second order condition involves a higher order polynomial, which is difficult to solve analytically, but which can be solved numerically for a given geometry.

With MALDI the two-stage source with first and second order velocity focusing provides very little improvement in resolution over that available with the single-stage source, but the two-stage source has the advantage that the focus can be adjusted electrically by varying the potential applied to the intermediate grid. By operating with a source length that is substantially shorter than that required for second order velocity focusing it is possible to obtain a broader focal range by sacrificing maximum resolving power at the focused mass. Calculated values of the resolving power limits R_{s1}^{-1} and R_{v2}^{-1} and the resultant resolving power R^{-1} for first order velocity focusing are plotted as a function of the voltage ratio y in Figure 3. In this case the two stages are taken of equal length so that $y = 2$ corresponds to a single stage source. As y increases a smaller fraction of the total accelerating voltage is applied across the first region in which the ions are produced. The spatial limit on resolving power increases monotonically with increasing y, whereas the velocity limit increases to a maximum and then decreases at large y values. On the other hand, at larger values of y the mass range of the focus is much narrower as shown in Figure 4.

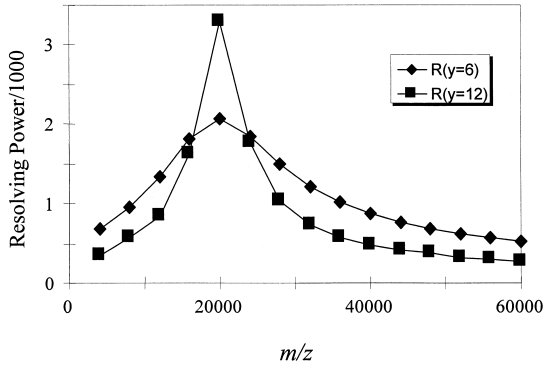

Figure 4. Calculated resolving power as function of mass-to-charge ratio for two values of the voltage ratio y for the analyzer defined in Figure 3 with first order focus at $m/z = 20{,}000$ and with an accelerating voltage of 20 kV.

Case IV. Two-Stage Source with Single-Stage Mirror

In this case the f coefficients are given by eqs 123–126 in the Appendix and the potential diagrams are shown in Figure 13b, c. If we let $r = 4d_R/D$, the conditions for first and second order spatial focusing are

$$2d_a/D = (1 - r)/y^{3/2} - (2d_0/D)[y^{1/2}/(y - 1)] \times (1/y - 1/y^{1/2}) \quad (46)$$

$$2d_0/D = 1 - r - (3 - r)/y \quad (47)$$

The condition for first order velocity focusing is given by eq 19, and the condition for second order velocity focusing, eq 21, can be solved numerically. For the MALDI case the two-stage source does not give significant improvement over the single-stage source operated at comparable mirror length with first and second order velocity focusing. However, the two-stage source does provide additional flexibility. For example, the same source can be used with both a linear and a reflecting analyzer, and the focus conditions can be varied to sacrifice ultimate resolution at a particular mass for adequate resolution over a broader mass range. This is the configuration we have chosen for application to MALDI, and its characteristics are discussed in more detail below.

Case V. Single-Stage Source with Two-Stage Mirror

In this case the f coefficients are given by eqs 136–139 in the Appendix and the corresponding potential diagrams are shown in Figure 13a, d. The conditions for first and second order spatial focusing are given by

$$4d_1/D = (w - 3)/w - (2d_a/D)(w - 1)/w \quad (48)$$

$$4d_2/D = (1 - 2d_a/D)/w^{3/2} + (4d_1/D)/(w + w^{1/2}) \quad (49)$$

where w is the ratio of the total accelerating voltage to the voltage difference applied across the second stage of the mirror. First order velocity focusing is obtained by satisfying eq 19, and the conditions for second order velocity focusing can be determined by numerically solving eq 21.

The two-stage mirror was first described by Mamyrin [10], and in his design the distance d_1 was much smaller than d_2. This design creates a situation in which the field strength is the first stage of the mirror is very high compared to that in the second stage. It has recently been shown [11] that scattering at the grids may seriously limit the resolution, and that better performance can be obtained in practice by employing a mirror design in which the lengths of the two stages are more nearly equal. It should also be noted that the same order of space focusing can be achieved using a two-stage source with a single-stage mirror. In MALDI, where velocity focusing is required, the only theoretical advantage for the two-stage mirror is that the physical length of the mirror may be shorter than for a single-stage mirror with comparable performance.

Case VI. Two-Stage Source with Two-Stage Mirror

The f coefficients for this case are given by eqs 144–147 in the Appendix, and the potential diagrams are shown in Figure 13b, d. First and second order focusing can be achieved by combining the conditions given above. It should also be theoretically possible to find a third order focusing condition since an additional free parameter is available, but unless the initial spread in position is very large this result is only of academic interest. If we focus the source at D_1 and the mirror at D_2, then the total drift space is

$$D = D_1 + D_2 \quad (50)$$

and the focusing conditions are given by

$$2d_0/D_1 = 1 - 3/y \quad (51)$$

$$2d_a/D_1 = 1/y^{3/2} + (2d_0/D_1)/(y + y^{1/2}) \quad (52)$$

$$4d_1/D_2 = 1 - 3/w \quad (53)$$

$$4d_2/D_2 = 1/w^{3/2} + (4d_1/D_2)/(w + w^{1/2}) \quad (54)$$

As in the other cases cited above, first order velocity focusing is obtained by satisfying eq 19, and the conditions for second order velocity focusing can be determined numerically by solving eq 21. Except possibly for physical size, there appears to be little advantage to this configuration for MALDI.

Higher Order Focusing

As has been discussed by Rockwood [12], it is theoretically possible to achieve space (energy) focusing to infinite order using a parabolic reflector with no field-free drift space. Cotter and co-workers [13] have described a curved-field reflector with approaches this ideal and allows improved resolution over a wide energy range. This system has been applied to the analysis of fragment ions produced by postsource decay (PSD) where the energy of low-mass fragment ions may be only a small fraction of that of the primary ions. First order velocity focusing with delayed extraction has been shown to be feasible with the curved-field reflector described by Cotter [13], but not for the idealized "Perfectron" described by Rockwood [12].

Other Limits on Resolution

With delayed extraction the contribution of initial velocity to measured peak width can be made very small for a selected ion of given mass-to-charge ratio, but the very high theoretical resolution is rarely achieved because other contributions then become dominant.

Time Measurement

At low values of mass-to-charge ratio the resolution is generally limited by the uncertainty in the TOF measurements. With MALDI, using a transient digitizer and a channel plate detector, the time resolution is limited by the width of a single ion pulse as measured by the digitizer. Using a dual channel plate with an impedance-matched anode, single-ion pulses 1.2 ns in width (FWHM) have been measured using a digitizer with a 0.25 ns bin width [14]. Because the flight time increases is proportion to the square root of the mass, and the uncertainty in the time measurement is independent of mass, the resolving power limit because of the time measurement increases in proportion to the square root of mass-to-charge ratio of the ion.

Trajectory Errors

The theoretical analysis of TOF analyzers given in the Appendix assumes that all of the electric fields are uniform and that the ion detector is a plane perpendicular to the ion velocity vector. This defines an ideal one-dimensional analyzer as an approximation to the real three-dimensional system. Any deviation from this ideal can lead to ions with the same nominal velocity having different trajectories through the system and, as a consequence, slightly different flight times. One obvious example of such a trajectory error is the channel plate detector which consists of small diameter channels inclined at a small angle to the normal to the nominal detector plane. Thus, the distance that an ion travels before striking the inside of the channel and producing secondary electrons depends on its position relative to the axis of the channel. The total variation in flight distance is given by

$$\Delta L = d / \sin \alpha \tag{55}$$

where d is the diameter of the channel and α is the angle of the channel axis relative to the ion velocity vector. The resolution limit because of this error is given by

$$R_L = d / Df_0 \sin \alpha \tag{56}$$

where it is assumed that the contribution (FWHM) to the peak width is one-half of the total variation given by eq 55. In the smaller reflecting instrument on which resolution enhancement by delayed extraction was first demonstrated [8], the detector employed a channel plate with a coaxial aperture and 25 μm diameter channels set at 8 degrees to the normal, and the effective flight path Df_0 was approximately 2 m. For this case the calculated resolving power limit because of the detector was about 11,000. By using a smaller channel diameter, a larger angle, or a larger overall instrument this resolving power limit can be increased.

Other trajectory errors may be introduced by field nonuniformity. Any focusing element designed to increase ion transmission by focusing the beam involves interchange between axial kinetic energy and transverse kinetic energy and may introduce significant trajectory errors. This generally implies a trade-off between ion signal intensity and resolving power similar to that observed in other mass analyzers.

Scattering at Grids

The uniform fields assumed in the theoretical model can only be approximated in practice by using fine mesh grids to separate regions of different electrical field strength. These grids cause a small loss in ion intensity because of scattering of ions from the grids, and under some conditions small angle scattering at the grids can degrade resolution. This problem has been elegantly treated by Bergmann et al. [11]. The major problem is that ions which pass near a grid wire may be deflected resulting in a change in the axial velocity, whereas ions that pass through the center of the grid opening are undeflected and continue with no change in axial velocity. Grids in the ion source or at the detector have a very small effect on resolution because the total distance traveled before (source) or after (detector) deflection is a small part of the total flight path. Grids in the mirror may cause a significant reduction in resolving power. The magnitude of the effect depends on the difference in field strength of the fields separated by the grid relative to the kinetic energy of the ions as they pass through the grid. This effect is particularly important in the two-stage mirror design of Mamyrin [10], but it can be substantially reduced by making the lengths of the two stages more nearly equal as de-

scribed by Bergmann et al. [11]. For a single-stage reflector the field strength is considerably less than in the two-stage case, and the only grid is at the mirror entrance where the kinetic energy is highest. In this case the perturbation to resolution is generally small compared to other trajectory errors such as described above.

High Voltage Variations

For a simple linear TOF analyzer the resolution limit because of fluctuations in the accelerating voltage is

$$R = \delta m/m = \delta V/V \tag{57}$$

where V is the accelerating voltage, and δV the fluctuations over a time period comparable to or longer than the ion flight time through the ion source. Faster fluctuations will be less significant because their effect is averaged out. Because power supplies with ripple and noise figures of 0.001% are commercially available, this should not be a serious limitation at resolving power below 100,000. For systems employing an ion mirror the resolution limit imposed by fluctuations in the mirror voltage is also given by eq 57, and the accelerating voltage is less critical.

Calibration and Mass Accuracy

In TOF mass spectrometry the flight time of ions is measured, and from those measured times the mass-to-charge ratios of the ions detected is determined. In the case of orthogonal injection of ions from an external source, the ratio of velocities v_0/v_n is normally independent of mass, so that eq 1 can be trivially inverted to give

$$(m/z)^{1/2} = A(t - t_0) \tag{58}$$

where t is the arrival time of the ion as determined with a digitizer, and t_0 is introduced to correct for the fact that the digitizer is not necessarily started at the same time that the extraction pulse is applied. If the instrumental parameters are accurately known, the calibration constant A can be determined by inverting eq 1; alternatively both A and t_0 can be determined experimentally by calibration measurements on two or more known ions. In the case of MALDI where the initial velocity is nearly independent of mass [15], the perturbations are mass dependent and accurate inversion of eq 1 is more complicated. For MALDI eq 1 can be arranged to the form

$$A(t - t_0) = (m/z)^{1/2}[1 - Bv_0(m/z)^{1/2} - Cv_0^2(m/z)] \tag{59}$$

The correction terms within the square bracket are small compared to unity, but not insignificant. Approximating mass-to-charge ratio in the correction terms by eq 58, this equation can be formally inverted to give

$$(m/z)^{1/2} = A(t - t_0)[1 + Bv_0A(t - t_0) + Cv_0^2A^2(t - t_0)^2] \tag{60}$$

This equation shows explicitly the dependence of the mass calibration on the average initial velocity v_0 up to second order. Higher order terms in the initial velocity are neglected, but this equation generally represents the exact expression with an error less than 1 ppm. Theoretical values for these calibration constants can be derived from eq 1. These are given by

$$A = [(2V)^{1/2}/Df_0][1 + (f_1/f_0)(v_0\Delta t/d_a) + (f_2/f_0)(v_0\Delta t/d_a)^2] \tag{61}$$

$$B = 2d_ay/Df_0(2V)^{1/2} \tag{62}$$

$$C = yf_1/2Vf_0 \tag{63}$$

where v_0 is the average initial velocity and SI units are used throughout. The calibration coefficients can be calculated with an accuracy limited only by the accuracy with which the instrumental parameters and the average initial velocity are known. This is normally adequate for a first approximation, but for more accurate work empirical calibration is required. One procedure is to calibrate on two or more known peaks to determine the major constants A and t_0, and to calculate the correction terms from the instrumental parameters, and the nominal value of the average initial velocity corresponding to the matrix used as described earlier [15]. An alternative procedure is to determine all four constants empirically using four or more known peaks. Either procedure gives excellent results provided the average initial velocities of calibrants and unknowns are all substantially the same. The latter procedure can be used to determine an experimental value for the average initial velocity. Systematic errors are often observed when the calibrants and unknowns are different types of ions, which may be formed by different mechanisms. For example, sodiated ions from polyethylene glycols do not work well as calibrants for protonated peptides, presumably because the average initial velocities are different.

Conclusions from Theoretical Considerations

1. First and second order velocity focusing is possible with a simple TOF analyzer consisting of either a single-stage or a two-stage source with a field-free flight tube. Very high theoretical resolving power can be obtained at a selected mass-to-charge ratio, but second order focusing with this simple analyzer

Table 1. Dimensions of instruments used for comparison with theory[a]

Instrument	1	2
Type	Linear Case III	Reflector Case IV
Source		
First region, d_a	3.6	2.8
Second region, d_0	17.4	17.4
Drift space, D	1292.0	1423.4
Reflector, d_R^0	n.a.	391.4

[a]All dimensions in mm.

is impractical for most applications because the range of focus is too narrow.

2. Addition of a mirror to the analyzer does *not* improve the theoretical resolution for the focused mass with first and second order velocity focusing, but it dramatically broadens the range of focus and improves the ease of accurate mass calibration.
3. An analyzer consisting of a two-stage source and single-stage mirror provides maximum flexibility and performance with MALDI. It can be used in first order mode to obtain a broad range of focus or in first and second order mode to give high resolving power at a selected mass with useful range of focus.
4. For velocity focusing there is no advantage in using a two-stage mirror. Scattering at the intermediate grid in a two-stage mirror may actually reduce the practical performance from that of the single-stage mirror.

Practical Analyzers for MALDI-TOF

Two mass analyzers have been employed for comparing experimental results with theoretical predictions. Critical dimensions of these instruments are summarized in Table 1. Instrument 1 is a simple linear analyzer with two-stage source, corresponding to Case III above, and Instrument 2 employs a single-stage reflector with a two-stage source, Case IV. A schematic diagram of Instrument 2 is shown in Figure 5. An earlier version of instrument 2 [8] used a coaxial geometry with two-stage source and single-stage mirror in which the detector was a 75 mm dual channel plate with a central aperture. These large detectors were only available with 25 μm diameter channels. After installing delayed extraction on this instrument, it became apparent that the resolution was limited by the detector. To correct this problem the mirror was inclined at an angle of 1 degree relative to the axis and the coaxial detector was replaced by a 40-mm-diameter DCP with 10 μm channels mounted off-axis as illustrated in Figure 5. With this new analyzer configuration the experimentally observed resolution is in good agreement with theoretical predictions. This system employs a two-stage source with dimensions indicated in Table 1 and includes a detector mounted behind the mirror which provides Case III operation with the mirror voltage turned off, and a

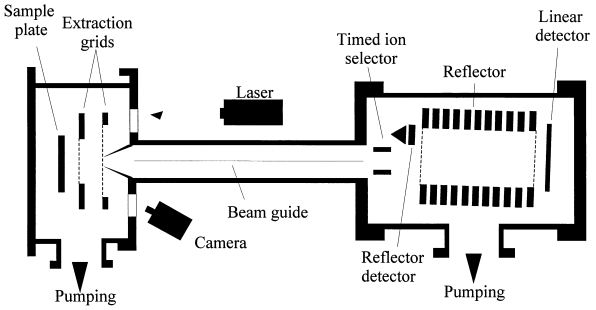

Figure 5. Schematic diagram of MALDI-TOF instrument employing a two-stage source and a single-stage mirror. Critical dimensions are given in Table 1. The axis of the mirror is inclined relative to the nominal direction of the incoming ion beam by 1 degree and the DCP detector for the reflected beam is adjacent to the exit from the mirror. A second DCP detector is located behind the mirror for use in the linear mode when the mirror voltage is turned off.

detector at the mirror exit, Case IV, with the mirror voltage applied. The physical length of the mirror is approximately 1.1 times larger than one quarter of the field-free drift length, so that for $r = 1$, in eq 31 for example, the voltage applied across the mirror is 10% higher than the accelerating voltage.

Comparison with Experimental Results

With Instrument 1 the relatively short source length employed does not allow second order focusing to be achieved, but as shown in Figure 6, there is a maximum in a plot of the resolving power as a function of the voltage ratio y. At the maximum resolving power the second order dependence on velocity is minimum, but not zero. Operating at this point provides a velocity resolving power limit significantly less than theoretically possible with second order focusing, but still

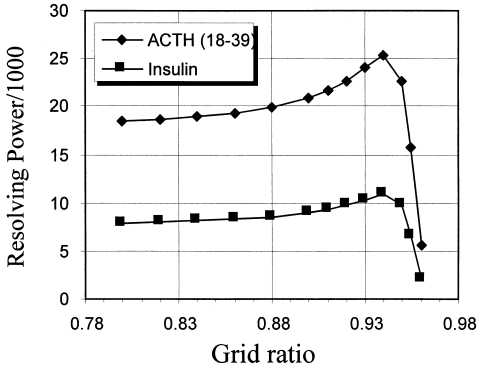

Figure 6. Calculated velocity resolving power limit R_{v2}^{-1} for instrument 1 with first order velocity focusing as a function of grid ratio for MH^+ of insulin, m/z 5734.5, and ACTH clip (18–39), m/z 2466. Accelerating voltage = 20 kV and assumed average initial velocity = 300 m/s. The grid ratio is the fraction of the total accelerating voltage applied to the intermediate grid separating the two regions of the two-field source, and is equal to $1 - 1/y$, where y is ratio of the total voltage to voltage applied across the first region.

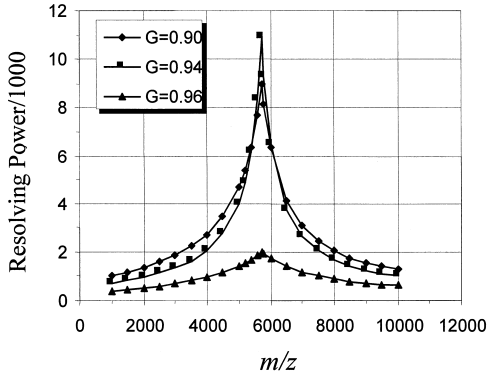

Figure 7. Calculated resolving power as a function of mass-to-charge ratio with first order velocity focusing for MH^+ of insulin at different grid ratios, G, for instrument 1. At each grid ratio the delay time is adjusted to correspond to first order velocity focus at m/z 5734.5.

sufficient that the actual resolving power is generally limited by other factors. Furthermore, the breadth of focus is considerably wider as shown in Figure 7 which may be contrasted with Figure 2 where resolving power as a function of mass is shown for a linear analyzer with second order focusing and similar field-free drift space dimensions. Examples of spectra obtained with optimized first order velocity focusing on Instrument 1 are shown in Figure 8. These were all obtained by operating the grid voltage at near the resolution maximum and adjusting only the delay time to optimize the resolution.

The optimum delay times determined experimentally are compared with theoretical calculations in Table 2. Delay times calculated from eq 19 differ by about a factor of 2 from those determined experimentally. A more accurate calculation of optimum delay time employing eq 22 reduces the disagreement, but only marginally. Optimum delay times have also been calculated "exactly" by calculating flight times as functions of initial velocity using the exact equation 116 in the Appendix and determining the optimum delay by simplex optimization. These "exact" results are in reasonable agreement with the approximate calculations, but not with experiment. It appears that this discrepancy is primarily because of the fact that the one-dimensional model does not represent the real three-dimensional system with sufficient accuracy. The calculations are based on the assumption of uniform electric fields, and small deviations in uniformity may cause the effective lengths of these fields to differ from their geometric lengths. The theoretical delay time is particularly sensitive to such errors.

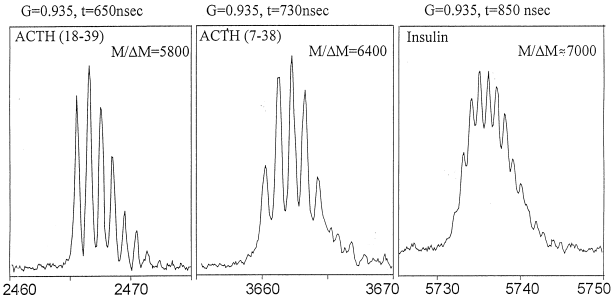

Figure 8. Examples of observed isotopic profiles for three masses under optimized first order focusing conditions for instrument 1. The grid ratio G was set near the theoretical optimum at 0.935 and the delay time was adjusted to optimize the resolution at each mass. Matrix: αCHCA, V = 20 kV.

Table 2. Optimum delay times for Instrument 1

	Delay, Δt (ns)			
m/z	1st approx.	2nd approx.	Exact	Experimental
2466	317	364	342	650
3661	386	448	423	730
5735	483	572	539	850

The calculated resolving power for this case is compared with the experimental results of Figure 8 in Table 3. The agreement between experimental and calculated results is excellent. As can be seen from Table 3, the spatial resolution limit R_{s1} is the most critical limit on resolution. The velocity limit becomes important at higher mass, and time resolution limit is more significant at lower mass. The experimental results represent the best that were achieved in several trials under the indicated conditions. In repetitive measurements the resolution varied by ~20%, presumably because of variations in effective widths of the distributions of initial velocity and/or position. At higher masses, isotopic resolution is not achieved with the linear analyzer, but peak widths approaching the width of the isotopic envelope are approached up to at least m/z 30,000.

With the reflecting instrument (Instrument 2 in Table 1) illustrated in Figure 5, resolving power of about 20,000 can be obtained for peptides and small proteins. Performance for proteins appears to be primarily limited by in-flight fragmentation. This instrument is particularly useful for analyzing protein digests where a wide range of focus and high mass accuracy over a broad range are important. The combination of a two-stage source with a single-stage mirror allows considerable flexibility in the tuning. The instrument may be tuned to provide maximum velocity resolving power at a particular mass, minimum dependence on initial velocity, or widest range of focus. Examples of three different tuning conditions are illustrated in Figure 9. In tuning #1 a relatively low value of the grid voltage,

Table 3. Calculated resolving power limits and comparison with experimental results for Instrument 1

m/z	q[a]	R_{v2}^{-1}	R_{s1}^{-1}[b]	R_t^{-1}[c]	R_{calc}^{-1}	R_{exp}^{-1}
2466	0.00757	24,800	7820	10,500	6080	5800
3661	0.00911	16,670	7820	12,800	6200	6400
5735	0.0114	10,650	7820	16,000	5870	7000

[a] δv_0 = 300 m/s.
[b] δx = 0.01 mm.
[c] δt = 1.6 ns.

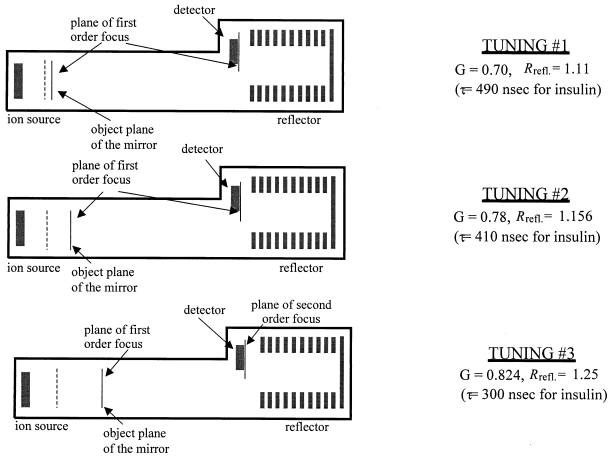

Figure 9. Schematic illustration of three different "optimum" tuning conditions for the instrument 1. In all cases the plane of first order focus for the source corresponds to the object plane for the reflector, and the beam is refocused, to first order, at the detector. In tuning 3, both first and second order velocity focusing are achieved at the detector.

corresponding to a small value of the voltage ratio, is used which produces a first order focus very close to the source, and the mirror voltage is lowered to refocus (first order) at the detector. In this case the focus is broad, but the maximum velocity resolving power at a selected mass is lower, and some dependence of resolving power on average velocity is expected for different matrices. In tuning #2 the first order focus is moved farther from the source by increasing the voltage ratio y, and in tuning #3 y is increased still further and the mirror voltage adjusted to provide second order focusing at the mirror. It might be expected that tuning #3 would give the highest resolving power at a selected mass, but unfortunately as we move closer to the second order velocity focus the space focus limit decreases and becomes dominant. Optimum delay times calculated from eq 19 and from the exact theory are compared with the experimentally determined values in Table 4. Except for tuning #1 the approximate calculations are in good agreement with the exact result and in fair agreement with experimental values. Tuning #1 corresponds to operating very near the first order space focusing point, that is, f_1 is very small. In this region it appears that neglecting higher order terms in the calculation of delay time produces a significant error. Calculated results for each of the resolving power limits

Table 4. Delay times for insulin MH^+ under tuning conditions of Figure 9

			Delay, Δt (ns)			
Tuning	y	r	1st approx.	2nd approx.	Exact	Experimental
#1	3.33	0.991	694	360	365	490
#2	4.55	0.952	392	330	335	410
#3	5.69	0.880	261	255	257	300

Table 5. Calculated resolving power limits for Instrument 2[a]

	R_v^{-1}						
	aCHCA		DHBs		R_s^{-1}	R_t^{-1}	
m/z	1296	5734	1296	5734	any	1296	5734
Tuning							
#1	10,300	50,400	7600	18,100	58,300	20,600	43,300
#2	8,700	148,000	5000	53,400	39,400	20,200	42,500
#3	7,200	298,000	4300	107,000	24,300	19,500	41,000

[a]The resolution limit due to trajectory errors, R_L is estimated to be 28,000.

are given in Table 5, and the resultant resolving power is compared with experiment in Table 6. In all cases the resolution was optimized for MH+ of insulin, and the resolution at angiotensin is a measure of the breadth of focus.

With tuning #2 the resolution at the selected mass is nearly independent of matrix because velocity resolution is not the limiting factor, and the effect of initial velocity on resolution is much less important. The resolution is limited by trajectory error and time resolution. Examples of insulin spectra obtained with three different matrices under identical tuning conditions are shown in Figure 10. As indicated in the figure, the average initial velocities determined earlier [15] are significantly different for these matrices, but as indicated theoretically, velocity resolution is not limiting with this tuning condition. With tuning #3 even higher velocity resolving power is predicted, but the space resolution now becomes limiting. Thus, the resolving power is independent of matrix but is lower because of the space resolution limitation. While tuning #1 shows more dependence on matrix it is generally preferred for the analysis of protein digests because it focuses over the broadest mass range and gives the smallest velocity dependent corrections in calibrating the mass scale. Examples of peptide spectra obtained in a single measurement are shown in Figure 11. In this case the focused mass was approximately 2500 u. The resolving power is greater than 10,000 over the range from roughly 1000 to 6000 u.

This velocity dependent corrections of the mass scale for these three tunings are summarized in Figure 12. For tuning #1, corresponding to the shortest focal length for the source, the velocity dependent corrections are

Table 6. Comparison of calculated resolving power with experimental results for Instrument 2[a]

	aCHCA		DHBs	
m/z	1296	5734	1296	5734
Tuning				
1	8700 (8000)	20,000 (19,000)	6800 (5000)	13,900 (15,000)
2	7500 (7000)	19,900 (20,000)	4700 (4500)	18,800 (19,500)
3	6400 (3500)	16,700 (15,500)	4100 (3000)	16,600 (16,000)

[a]Experimental values are in parentheses.

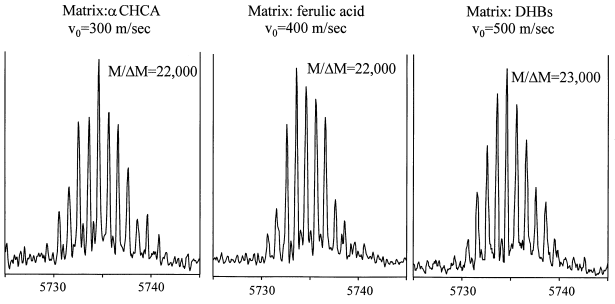

Figure 10. Examples of insulin spectra obtained with tuning #2 using different matrices.

smallest, and for tuning #3, where a longer source focal length allows second order velocity focusing the corrections are largest. This leads to the seemingly paradoxical conclusion that better velocity focusing and higher theoretical resolving power at a selected mass does not imply better mass accuracy. Instead a tuning condition that minimizes the effect of mass on resolution also minimizes the correction terms that are dependent on initial velocity. Tuning with a short source focal length also minimizes the effect of ion initial position on the flight time. Because initial velocity and position are variables not under direct experimental control, these are the major sources of uncontrolled variations in ion flight times, and hence the limiting factors in achieving ultimate mass accuracy with either internal or external calibration. Thus tuning 1 is preferred for obtaining the most accurate mass measurements, even though the maximum resolution may be somewhat less than can be obtained with other operating conditions.

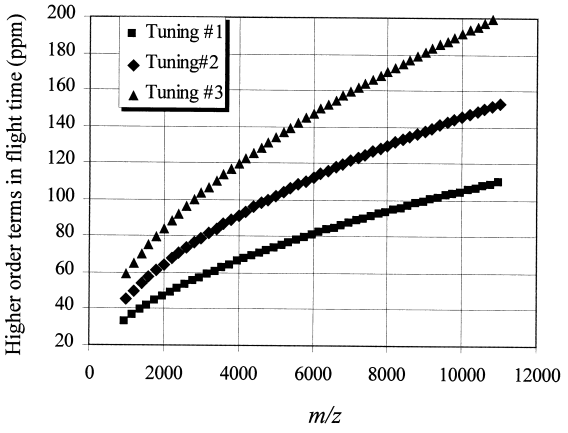

Figure 12. Calculated deviation from the simple TOF calibration law that time is proportional to square root of mass for the three tuning conditions defined in Figure 9. Values are plotted as the negative deviation as predicted by eq 60.

Conclusions

A mathematical model accurately describing the behavior of TOF analyzers employing uniform electrical fields has been presented. This model has been applied to accurately evaluating the limits on resolution and mass accuracy for various instrumental geometries. Particular emphasis has been placed on techniques appropriate for use with MALDI where velocity focusing is necessary for achieving high performance, but the techniques described are also applicable to other ion introduction methods, such as orthogonal injection, where space focusing may be more important. It was found that first

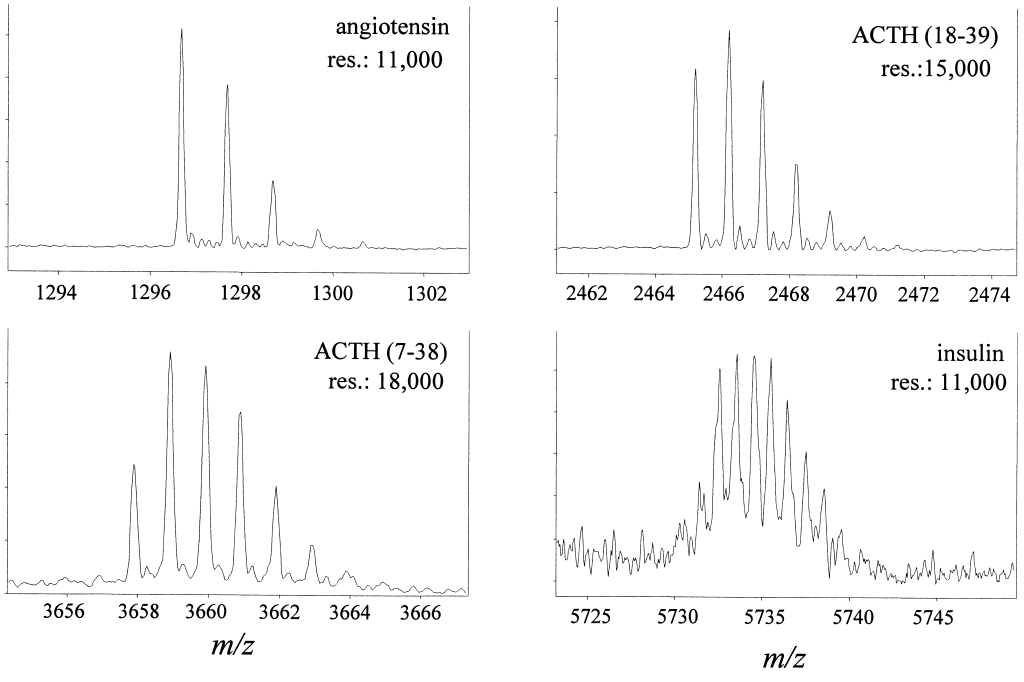

Figure 11. Peak profiles for several masses from a single spectrum obtained using tuning #1 with the delay time set for optimum resolution at $\sim m/z = 2500$.

and second order velocity focusing is possible with the simplest delayed extraction TOF analyzer imaginable; that is, one consisting only of a single-field source and a field-free drift space, and that quite high resolution at a selected mass is theoretically possible with this simple system. Unfortunately, use of this analyzer at second order focus appears to be impractical both because the resolution as a function of mass is very sharply peaked at the focused mass and because the tuning can only be done mechanically. Addition of a single-stage mirror provides an additional free parameter, the length of the mirror, which can be adjusted electrically by varying the voltage applied to the mirror. This is a practical system which can be readily optimized for any given distributions of initial velocities and positions, and has the advantage that all of its performance characteristics can be readily calculated. Addition of the mirror does not increase the theoretical resolution of a system employing velocity focusing, rather for the same length drift space it decreases the resolution; but it dramatically broadens the range of focus and allows more accurate mass calibration by decreasing the effect of initial velocity and position on the ion flight times. Replacing the single-stage source with a two-stage source does not necessarily provide higher performance, but it provides an additional degree of freedom and hence more flexibility. In particular, it allows the same source to be optimized for both linear and reflecting analyzers in the same instrument. We were unable to find any advantages for two-stage or higher order mirrors with velocity focusing.

The mathematical model has been applied to optimizing the performance of both linear and reflecting analyzers for applications to MALDI, and calculated performance under different tuning conditions has been compared with experimental results. In general, calculated resolutions are in good agreement with experiment indicating that the major factors limiting the resolution are accurately described by the model. In general we find that the most useful operating conditions are those that provide sufficient resolution over a broad range of mass with minimal dependence of the mass scale on initial velocity, even though the resolution may be significantly less than the maximum that can be achieved for a limited mass range. Calculations of optimum delay times are less satisfactory. In some cases the agreement with experiment is improved by determining the optimum delay using the exact equations for TOF, but most of the observed discrepancies appear to reflect deviations from the uniform fields assumed in the model.

Appendix I. Fundamental Theory

Equations from Basic Physics

1. Newton's second law. Force = Mass × Acceleration.

Acceleration is equal to the rate of change of the velocity, dv/dt. For charged particles in an electric field, force is charge z multiplied by electric field strength E, and the field is equal to the gradient of the potential. In general, acceleration, velocity, force, and electric field are vectors, but in the case of uniform fields the field is nonzero only in one direction. In this one dimensional case, we have

$$F = ma \text{ (Newton's law)} \tag{64}$$

$$F = zE \text{ (Force on a charged particle)} \tag{65}$$

$$E = V/d \text{ (uniform field, potential difference } V \text{ across distance } d \tag{66}$$

$$a = dv/dt \text{ (definition of acceleration)} \tag{67}$$

$$dv = adt \tag{68}$$

Integrating

$$v_2 - v_1 = at$$

or

$$t = (v_2 - v_1)/a \tag{69}$$

where v_2 is the final velocity after acceleration, v_1 is the initial velocity before acceleration, and t is the time that the ion spends in the field. In a field-free space, the acceleration is zero, and we have

$$v = dx/dt = \text{constant},$$

and integrating gives

$$t = (x_2 - x_1)/v = D/v \tag{70}$$

2. Conservation of energy. In conservative systems (i.e., no frictional losses) the sum of kinetic energy and potential energy is constant. For motion of charged particles in an electric field, this can be expressed as

$$T_2 - T_1 = z(V_1 - V_2) \tag{71}$$

where the kinetic energy $T = mv^2/2$. This can be solved for v to give an explicit expression for the velocity of a charged particle at any point.

For ions traveling through a series of uniform electrical fields the above equations provide exactly the TOF as a function of mass, charge, potentials, and distances. If the SI system is used, in which distance is expressed in meters, potentials in volts, masses in kg, charge in coulombs, and time in seconds, then no additional constants are required.

Case I. Single-Field Source

This is the simplest form of TOF analyzer. A uniform electric field is formed by applying a potential difference V to a pair of parallel plates spaced a distance d_a

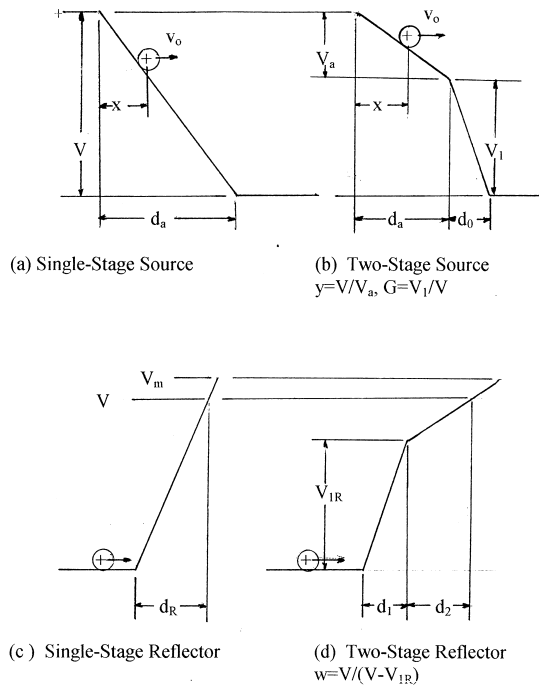

Figure 13. Potential diagrams for ion sources and reflectors. In a linear TOF analyzer, ions exiting the source travel a distance D through a field-free region to the detector. In reflecting analyzers the detector is positioned to receive ions after exiting the mirror, and the distance D is the total ion path length in the field-free region between source and detector.

apart. The potential diagram is shown in Figure 13a. One of the plates includes an aperture covered by a fine grid so that ions can pass from the accelerating region into the field-free drift space. A detector is located at a distance D from the apertured plate. Ions are produced at a point x in the field with initial velocity v_0, and the positive direction for both x and v_0 is taken in the direction of ion acceleration.

From conservation of energy the kinetic energy after acceleration (at $V = 0$) is given by

$$T(x, v_0) = mv^2/2 = T_0 + zV(d_a - x)/d_a = zV(1 - x/d_a + T_0/zV) \quad (72)$$

where

$$T_0 = mv_0^2/2 \quad (73)$$

Equation 72 can be simplified by defining a perturbation p given by

$$p = [T(0, 0) - T(x, v_0)]/T(0, 0) = x/d_a - T_0/zV \quad (74)$$

$$T(x, v_0) = mv^2/2 = zV(1 - x/d_a + T_0/zV) = zV(1 - p) \quad (75)$$

Solving for the velocity gives

$$v = (2zV/m)^{1/2}(1 - p)^{1/2} \quad (76)$$

The velocity of an ion originating from $x = 0$ with zero initial velocity is given by

$$v_n = (2zV/m)^{1/2} \quad (77)$$

And the perturbation p can be expressed in terms of the velocities as

$$p = x/d_a - T_0/zV = x/d_a - (v_0/v_n)^2 \quad (78)$$

In terms of these parameters the velocity is given by

$$v = v_n(1 - p)^{1/2} \quad (79)$$

From the basic equations 64–66 the acceleration is given by

$$a = F/m = zE/m = zV/md_a \quad (80)$$

Thus the time of flight through the acceleration region is given by

$$t_1 = v/a - v_0/a = (zV/md_a)^{-1}(2zV/m)^{1/2} \times (1 - p)^{1/2} - (zV/md_a)^{-1}v_0 \quad (81)$$

$$t_1 = (2d_a/v_n)[(1 - p)^{1/2} - v_0/v_n] \quad (82)$$

The flight time through the field-free drift tube to the detector is

$$t_2 = D/v = (D/v_n)[(1 - p)^{-1/2}] \quad (83)$$

The total flight time is the sum of these two contributions

$$t = t_1 + t_2 = (D/v_n)[(1 - p)^{-1/2} + (2d_a/D) \times (1 - p)^{1/2} - (2d_a/D)(v_0/v_n)] \quad (84)$$

For all cases of practical importance the perturbation p is small compared to unity. This allows the exact expression to be approximated accurately by expanding the terms inside the radicals in a power series and retaining as many terms as are required to achieve the desired degree of accuracy. The pertinent expansions are

$$(1 - p)^{-1/2} = 1 + p/2 + 3p^2/8 + 5p^3/16 + 35p^4/128 + \cdots \quad (85)$$

$$(1 - p)^{1/2} = 1 - p/2 - p^2/8 - p^3/16 - 5p^4/128 - \cdots \quad (86)$$

Expanding to fourth order and collecting terms we have

$$t = (Df_0/v_n)[1 + f_1p/f_0 + f_2p^2/f_0 + f_3p^3/f_0 + f_4p^4f_0 + \cdots - (2d_a/f_0D)(v_0/v_n)] \quad (87)$$

where

$$f_0 = 1 + 2d_a/D \quad (88)$$

$$f_1 = [1 - 2d_a/D]/2 \quad (89)$$

$$f_2 = [3 - 2d_a/D]/8 \quad (90)$$

$$f_3 = [5 - 2d_a/D]/16 \quad (91)$$

$$f_4 = 5[7 - 2d_a/D]/128 \quad (92)$$

and p is given by eq 78 above.

Case II. Single-Field Source Plus Single-Field Mirror

The potential diagram for a single-field mirror is shown in Figure 13c. The time of flight through a single-field mirror is given by

$$t = 2v/a_R \quad (93)$$

where v is the velocity of an ion entering the mirror, and a_R is the acceleration within the mirror. At the turning point in the mirror the velocity is zero and the time required to traverse from entrance to turning point is equal to the time from turning point to exit.

The velocity at the entrance to the mirror is the same as that in the drift tube, given by eq 79, and the acceleration in the mirror is

$$a_R = zV/md_R = v_n^2/2d_R \quad (94)$$

where d_R is the length of the mirror across which the potential difference V is applied. The TOF through the mirror is then

$$t_R = 2v/a_R = (D/v_n)(4d_R/D)[(1 - p)^{1/2}] \quad (95)$$

The total flight time is given by the sum of the contributions from the source, drift space, and mirror. This is given by

$$t = t_1 + t_2 + t_R = (D/v_n)[(1 - p)^{-1/2} + (2d_a/D + 4d_R/D)(1 - p)^{1/2} - (2d_a/D)(v_0/v_n] \quad (96)$$

Expanding in a power series in p the exact equation is approximated by eq 87 with the addition of the term, $4d_R/D$ into the expressions for the f coefficients, which become

$$f_0 = 1 + 4d_R/D + 2d_a/D \quad (97)$$

$$f_1 = [1 - 4d_R/D - 2d_a/D]/2 \quad (98)$$

$$f_2 = [3 - 4d_R/D - 2d_a/D]/8 \quad (99)$$

$$f_3 = [5 - 4d_R/D - 2d_a/D]/16 \quad (100)$$

$$f_4 = 5[7 - 4d_R/D - 2d_a/D]/128 \quad (101)$$

Case III. Two-Field Source

The potential diagram for a two-field source is shown in Figure 13b. In this case there is an intermediate grid in the ion accelerator with potential V_1 applied to that grid. As indicated in the potential diagram the length of the first acceleration region is d_a, and the length of the second acceleration region is d_0. The time in the first region, according to eq 69, is given by

$$t_1 = v_1/a_1 - v_0/a_1$$

From conservation of energy the kinetic energy after acceleration in the first region is given by

$$T_1(x, v_0) = mv_1^2/2 = T_0 + z(V - V_1)(d_a - x)/d_a = z(V - V_1)[1 - x/d_a + T_0/z(V - V_1)] \quad (102)$$

Where the initial kinetic energy T_0 is given by eq 73. If we define the voltage ratio y as

$$y = V/(V - V_1) \quad (103)$$

And the perturbation p as

$$p = [T_1(0, 0) - T_1(x, v_0)]/T_1(0, 0) = x/d_a - yT_0/zV \quad (104)$$

Then

$$T_1(x, v_0) = mv_1^2/2 = z(V/y)(1 - p) \quad (105)$$

Solving for the velocity gives

$$v_1 = (2zV/ym)^{1/2}(1 - p)^{1/2} \quad (106)$$

The acceleration in the first region of the source is given by

$$a_1 = z(V - V_1)/md_a = zV/ymd_a \quad (107)$$

Thus the flight time through the first acceleration region is given by

$$t_1 = v_1/a - v_0/a = (zV/ymd_a)^{-1}(2zV/ym)^{1/2} \times (1 - p)^{1/2} - (zV/ymd_a)^{-1}v_0 \quad (108)$$

$$t_1 = (2d_a/v_n)[y^{1/2}(1 - p)^{1/2} - yv_0/v_n] \quad (109)$$

The flight time through the second acceleration region is given by

$$t_2 = v/a_2 - v_1/a_2 \tag{110}$$

The kinetic energy after the second stage of accelerations is given by

$$\begin{aligned} T(x, v_0) &= T_1(x, v_0) + zV_1 = mv^2/2 \\ &= z(V/y)(1 - p) + z(y - 1)V/y \\ &= zV(1 - p/y) \end{aligned} \tag{111}$$

Solving for the velocity gives

$$v = v_n(1 - p/y)^{1/2} \tag{112}$$

where v_n is given by eq 77. The acceleration in the second region is given by

$$a_2 = zV_1/md_0 = zV(y - 1)/ymd_0 \tag{113}$$

and

$$t_2 = (2d_0/v_n)\{[y/(y - 1)][(1 - p/y)^{1/2} - (1 - p)^{1/2}/y^{1/2}]\} \tag{114}$$

The flight time through the field free region is given by

$$t_3 = D/v = (D/v_n)[(1 - p/y)^{-1/2}] \tag{115}$$

The total flight time is then given by

$$\begin{aligned} t = t_1 + t_2 + t_3 = (D/v_n)\{&(1 - p/y)^{-1/2} + (2d_0/D)[y/(y - 1)]\}(1 - p/y)^{1/2} \\ &+ y^{1/2}[2d_a/D + (2d_0/D)/(y - 1)](1 - p)^{1/2} - (2d_a/D)(v_0/v_n)) \end{aligned} \tag{116}$$

Expanding the radicals into power series in p and p/y and collecting coefficients, this exact equation can be approximated by

$$\begin{aligned} t = (Df_0/v_n)[1 &+ f_1p/f_0 + f_2p^2/f_0 \\ &+ f_3p^3/f_0 + \cdots - (2d_ay/f_0D)(v_0/v_n)] \end{aligned} \tag{117}$$

which is formally identical to eq 87, except for the factor of y in the last term and in the definition of p. In this case the coefficients are given by

$$\begin{aligned} f_0 = 1 &+ 2d_ay^{1/2}/D + (2d_0/D) \\ &\times [y/(y - 1)](1 - 1/y^{1/2}) \end{aligned} \tag{118}$$

$$\begin{aligned} f_1 = \{&1/y - 2d_ay^{1/2}/D - (2d_0/D) \\ &\times [y/(y - 1)](1/y - 1/y^{1/2})\}/2 \end{aligned} \tag{119}$$

$$\begin{aligned} f_2 = \{&3/y^2 - 2d_ay^{1/2}/D - (2d_0/D)[y/(y - 1)] \\ &\times (1/y^2 - 1/y^{1/2})\}/8 \end{aligned} \tag{120}$$

$$\begin{aligned} f_3 = \{&5/y^3 - 2d_ay^{1/2}/D - (2d_0/D)[y/(y - 1)] \\ &\times (1/y^3 - 1/y^{1/2})\}/16 \end{aligned} \tag{121}$$

Fourth and higher order terms can be easily added if necessary, but except in cases where p approaches 0.1 or higher the error introduced by truncating the series after the third order term is small compared to errors due to deviations from the one-dimensional model.

Case IV. Two-Field Source Plus Single-Field Mirror

The potential diagrams for this case are shown in Figure 13b, c. In this case the acceleration is given by eq 94 and the velocity entering the mirror by eq 112. Thus, the time through the mirror is given by

$$t_R = 2v/a_R = (D/v_n)(4d_R/D)[(1 - p/y)^{1/2}] \tag{122}$$

The exact equation for TOF is obtained by adding the time in the mirror to that for the source and drift space given by eq 116 above. The approximate expression is given by 117 with a term due to the mirror added to the f coefficients. These then become

$$\begin{aligned} f_0 = 1 &+ 4d_R/D + 2d_ay^{1/2}/D + (2d_0/D) \\ &\times [y/(y - 1)](1 - 1/y^{1/2}) \end{aligned} \tag{123}$$

$$\begin{aligned} f_1 = \{&(1 - 4d_R/D)/y - 2d_ay^{1/2}D - (2d_0/D) \\ &\times [y/(y - 1)](1/y - 1/y^{1/2})\}/2 \end{aligned} \tag{124}$$

$$\begin{aligned} f_2 = \{&(3 - 4d_R/D)y^2 - 2d_ay^{1/2}/D - (2d_0/D) \\ &\times [y/(y - 1)](1/y^2 - 1/y^{1/2})\}/8 \end{aligned} \tag{125}$$

$$\begin{aligned} f_3 = \{&(5 - 4d_R/D)/y^3 - 2d_ay^{1/2}/D - (2d_0/D) \\ &\times [y/(y - 1)](1/y^3 - 1/y^{1/2})\}/16 \end{aligned} \tag{126}$$

Case V. Single-Field Source Plus Two-Field Mirror

The potential diagrams are shown in Figure 13a, d. In this case there is an intermediate grid in the ion reflector with potential V_{1R} applied to that grid. As indicated in the potential diagram the length of the first region is d_1, and the length of the second acceleration region is d_2. The analysis of the two-field mirror is essentially identical to that for the two-field source except that the ions enter and exit the mirror with a velocity determined by the source, and the velocity at the turning point in the

second region is zero. Thus, the time in the second region is given by

$$t_{2R} = 2v_{1R}/a_{2R} \tag{127}$$

And the time in the first region is given by

$$t_{1R} = v/a_{1R} - v_{1R}/a_{1R} \tag{128}$$

The accelerations are

$$a_{1R} = zV_{1R}/md_1 = zV(w-1)/wmd_1 \tag{129}$$

$$a_{2R} = z(V - V_{1R})/md_2 = zV/wmd_2 \tag{130}$$

where

$$w = V/(V - V_{1R}) \tag{131}$$

The velocity at the entrance to the mirror v is given by eq 79 and the kinetic energy at the intermediate grid is

$$\begin{aligned} T_{1R}(x, v_0) = mv_{1R}^2/2 &= T(x, v_0) - zV_{1R} \\ &= zV(1-p) - zV(w-1)/w \\ &= zV(1-pw)/w \end{aligned} \tag{132}$$

where $T(x, v_0)$ for the single-field source is given by eq 75. Solving for the velocity gives

$$\begin{aligned} v_{1R} &= (2zV/wm)^{1/2}(1-pw)^{1/2} \\ &= v_n(1-pw)^{1/2}/w^{1/2} \end{aligned} \tag{133}$$

where v_n is given by eq 77. The flight times through the two sections of the mirror are then given by

$$\begin{aligned} t_{1R} = (4d_1/v_n)\{[w/(w-1)][(1-p)^{1/2} \\ - (1-wp)^{1/2}/w^{1/2}]\} \end{aligned} \tag{134}$$

$$t_{2R} = (4d_2/v_n)w^{1/2}(1-wp)^{1/2} \tag{135}$$

Adding the reflector flight times to those for the single-stage source and drift space given by eq 84 above provides an exact expression for this case. Expanding in power series and collecting terms, the exact expression can be approximated by eq 87 with terms due to the two-stage mirror added to the f coefficients. These are given by

$$\begin{aligned} f_0 = 1 + 2d_a/D + 4d_2w^{1/2}/D + (4d_1/D) \\ \times [w/(w-1)](1 - w^{-1/2}) \end{aligned} \tag{136}$$

$$\begin{aligned} f_1 = \{1 - 2d_a/D - 4d_2w^{3/2}/D - (4d_1/D) \\ \times [w/(w-1)](1 - w^{1/2})\}/2 \end{aligned} \tag{137}$$

$$\begin{aligned} f_2 = \{3 - 2d_a/D - 4d_2w^{5/2}/D - (4d_1/D) \\ \times [w/(w-1)](1 - w^{3/2})\}/8 \end{aligned} \tag{138}$$

$$\begin{aligned} f_3 = \{5 - 2d_a/D - 4d_2w^{7/2}/D - (4d_1/D) \\ \times [w/(w-1)](1 - w^{5/2})\}/16 \end{aligned} \tag{139}$$

Case VI. Two-Field Source Plus Two-Field Mirror

The potential diagrams are shown in Figure 13b, d. The exact equation for TOF is given by the sum of the time for the two-stage source and drift tube, eq 116 plus the contributions from the mirror. In this case the velocity at the entrance to the mirror v is given by eq 112 and the kinetic energy at the intermediate grid is

$$\begin{aligned} T_{1R}(x, v_0) = mv_{1R}^2 2 &= T(x, v_0) - zV_{1R} \\ &= zV(1 - p/y) - zV(w-1)/w \\ &= zV(1 - pw/y)/w \end{aligned} \tag{140}$$

where $T(x, v_0)$ for the two-field source is given by eq 111. Solving for the velocity gives

$$\begin{aligned} v_{1R} &= (2zV/wm)^{1/2}(1 - pw/y)^{1/2} \\ &= v_n(1 - pw/y)^{1/2}/w^{1/2} \end{aligned} \tag{141}$$

where v_n is given by eq 77. The flight times through the two sections of the mirror are then given by

$$\begin{aligned} t_{1R} = (4d_1/v_n)\{[w/(w-1)][(1 - pw/y)^{1/2} \\ - (1 - pw/y)^{1/2}/w^{1/2}]\} \end{aligned} \tag{142}$$

$$t_{2R} = (4d_2/v_n)w^{1/2}(1 - pw/y)^{1/2} \tag{143}$$

This exact equation can be approximated by eq 117 with the f coefficients given by

$$\begin{aligned} f_0 = 1 + 2d_a y^{1/2}/D + (2d_0/D)[y/(y-1)] \\ \times (1 - 1/y^{1/2}) + 4d_2w^{1/2}/D + (4d_1/D) \\ \times [w/(w-1)](1 - 1/w^{1/2}) \end{aligned} \tag{144}$$

$$\begin{aligned} f_1 = \{(1/y - 2d_a y^{1/2}/D - (2d_0/D)[y/(y-1)] \\ \times (1/y - 1/y^{1/2}) - 4d_2w^{3/2}/yD - (4d_1/D) \\ \times [w/(w-1)](1/y - w^{1/2}/y)\}/2 \end{aligned} \tag{145}$$

$$\begin{aligned} f_2 = \{(3/y^2 - 2d_a y^{1/2}/D - (2d_0/D)[y/(y-1)] \\ \times (1/y^2 - 1/y^{1/2}) - 4d_2w^{5/2}/y^2D - (4d_1/D) \\ \times [w/(w-1)](1/y^2 - w^{3/2}/y^2)\}/8 \end{aligned} \tag{146}$$

$$f_3 = \{(5/y^3 - 2d_a y^{1/2}/D - (2d_0/D)[y/(y-1)] \times (1/y^3 - 1/y^{1/2}) - 4d_2 w^{7/2}/y^3 D - (4d_1/D) \times [w/(w-1)](1/y^3 - w^{5/2}/y^3)\}/16 \quad (147)$$

The equations for the two-stage source reduce to those for the single-stage source when

$$y = 1,\ d_0 = 0 \quad (148)$$

or alternatively when

$$y = 1 + d_0/d_a \quad (149)$$

and the total acceleration distance becomes $d_0 + d_a$. Similarly, the two-stage mirror reduces to an equivalent one-stage mirror when

$$w = 1,\ d_1 = 0 \quad (150)$$

or when $w = 1 + d_1/d_2$ and the total reflection distance becomes

$$d_1 + d_2. \quad (151)$$

References

1. Karas, M.; Hillenkamp, F. *Anal. Chem.* **1988,** *60*, 2299–2301.
2. Beavis, R. C.; Chait, B. T. *Rapid Commun. Mass Spectrom.* **1989,** *3*, 233–236.
3. Beavis, R. C.; Chait, B. T. *Anal. Chem.* **1990,** *62*, 1836–1840.
4. Zhou, J.; Ens, W.; Standing, K.; Verentchikov, A. *Rapid Commun. Mass Spectrom.* **1992,** *6*, 671–678.
5. Brown, R. S.; Lennon, J. J. *Anal. Chem.* **1995,** *67*, 1998–2003.
6. Colby, S.; King, T. B.; Reilly, J. P. *Rapid Commun. Mass Spectrom.* **1994,** *8*, 865–868.
7. Whittal, R. M.; Li, L. *Anal. Chem.* **1995,** *67*, 1950–1954.
8. Vestal, M. L.; Juhasz, P.; Martin, S. A. *Rapid Commun. Mass Spectrom.* **1995,** *9*, 1044–1050.
9. Wiley, W. C.; McLaren, I. H. *Rev. Sci. Instrum.* **1955,** *26*, 1150–1157.
10. Mamyrin, B. A.; Karataev, V. I.; Shmikk, D. V.; Zagulin, V. A. *Sov. Phys. JETP* **1973,** *37*, 45–48.
11. Bergmann, T.; Martin, T. P.; Schaber, H. *Rev. Sci. Instrum.* **1989,** *60*, 347–349.
12. Rockwood, A. L. *34th Annual Conference on Mass Spectrometry and Allied Topics*; Cincinnati, OH, 1986.
13. Cornish, T. J.; Cotter, R. J. *Rapid Commun. Mass Spectrom.* **1994,** *8*, 781–785. Worral, T. A.; Cotter, R. J. *45th Annual Conference on Mass Spectrometry and Allied Topics*; Palm Springs, CA, 1997; p 1213.
14. Tektronix Model TDS 784A, Tektronix, Inc. Beaverton, OR.
15. Juhasz, P.; Vestal, M. L.; Martin, S. A. *J. Am. Soc. Mass Spectrom.* **1997,** *8*, 209–217.